nature neuroscience

SIRT1 collaborates with ATM and HDAC1 to maintain genomic stability in neurons

Matthew M Dobbin[1–3,9], Ram Madabhushi[1–3,9], Ling Pan[1–3], Yue Chen[4,5], Dohoon Kim[6], Jun Gao[1–3,8], Biafra Ahanonu[1–3], Ping-Chieh Pao[1–3], Yi Qiu[7], Yingming Zhao[4,5] & Li-Huei Tsai[1–3]

Defects in DNA repair have been linked to cognitive decline with age and neurodegenerative disease, yet the mechanisms that protect neurons from genotoxic stress remain largely obscure. We sought to characterize the roles of the NAD$^+$-dependent deacetylase SIRT1 in the neuronal response to DNA double-strand breaks (DSBs). We found that SIRT1 was rapidly recruited to DSBs in postmitotic neurons, where it showed a synergistic relationship with ataxia telangiectasia mutated (ATM). SIRT1 recruitment to breaks was ATM dependent; however, SIRT1 also stimulated ATM autophosphorylation and activity and stabilized ATM at DSB sites. After DSB induction, SIRT1 also bound the neuroprotective class I histone deacetylase HDAC1. We found that SIRT1 deacetylated HDAC1 and stimulated its enzymatic activity, which was necessary for DSB repair through the nonhomologous end-joining pathway. HDAC1 mutations that mimic a constitutively acetylated state rendered neurons more susceptible to DNA damage, whereas pharmacological SIRT1 activators that promoted HDAC1 deacetylation also reduced DNA damage in two mouse models of neurodegeneration. We propose that SIRT1 is an apical transducer of the DSB response and that SIRT1 activation offers an important therapeutic avenue in neurodegeneration.

Once formed during early development, neurons are retained for life and are therefore faced with the challenge of maintaining a stable genome for long periods of time. DNA damage, which perturbs genomic stability, has been linked to cognitive decline in the aging human brain[1], and mutations in DNA-repair genes manifest profoundly with neurological implications[2]. Recent studies have suggested that DNA damage is also elevated in disorders such as Alzheimer's disease and amyotrophic lateral sclerosis[3–5]. However, the precise mechanisms connecting DNA damage with neurodegeneration remain poorly understood.

Sirtuins are NAD$^+$-dependent lysine deacetylases that modulate a number of biological processes that are highly relevant to aging and neurodegeneration[6]. We previously reported that overexpression of SIRT1, the archetypal mammalian sirtuin, confers protection against neuronal loss in the transgenic CK-p25 mouse model of neurodegeneration[7]; however, the mechanisms underlying this protection were unclear. CK-p25 mice express a truncated fragment of the CDK5-activating partner, p35, in an inducible and forebrain-specific manner[8], and p25 induction systematically recapitulates various neurodegenerative pathologies, including the accumulation of amyloid-β peptides, neurofibrillary tau tangles, reduced synaptic density and neuronal atrophy in the forebrain[8,9]. Notably, further characterization of CK-p25 mice revealed that the occurrence of DSBs precedes all other pathological symptoms in these mice[10]. To understand how SIRT1 is able to suppress neuronal loss, we directly characterized the functions of SIRT1 in the neuronal DNA DSB response.

RESULTS

SIRT1 is essential for DSB signaling and DNA repair in neurons

To determine whether SIRT1 is essential for genomic stability in neurons, we transduced neurons cultured from mouse embryos carrying *loxP*-flanked *Sirt1* (*Sirt1*$^{loxP/loxP}$) with a lentiviral vector carrying Cre recombinase tagged with enhanced GFP (Cre-eGFP) to delete *Sirt1* (**Supplementary Fig. 1a**) and assessed DNA damage using a single-cell electrophoresis assay (comet assay)[11]. A significant fraction of *Sirt1*$^{loxP/loxP}$ neurons transduced with Cre-eGFP (hereafter referred to as *Sirt1* knockout neurons) showed comet tails even without treatment with an exogenous DNA-damaging agent (**Fig. 1a**). In the presence of the DSB-inducing drug etoposide, *Sirt1* knockout neurons had longer 'tail moments' compared to controls transduced with a vector carrying nonfunctional Cre (eGFP) (**Fig. 1a**). These results suggest that neurons lacking SIRT1 are more susceptible to DNA damage. In addition, whereas the tail moments in etoposide-treated control neurons were significantly reduced after recovery for 16 h, *Sirt1* knockout neurons continued to have long comet tails, suggesting that *Sirt1* knockout neurons are also deficient in DSB repair (**Fig. 1a**). To verify this, we used a reporter assay system (**Supplementary Fig. 1b**,**c**)[12] in which reconstitution of a functional GFP gene indicates successful DSB repair through the nonhomologous end-joining (NHEJ) pathway. In this assay, the number of GFP$^+$ neurons was significantly reduced after SIRT1 knockdown (**Fig. 1b**), confirming that SIRT1 is necessary for NHEJ-mediated DSB repair in neurons.

[1]Picower Institute for Learning and Memory, Massachusetts Institute of Technology (MIT), Cambridge, Massachusetts, USA. [2]Department of Brain and Cognitive Sciences, MIT, Cambridge, Massachusetts, USA. [3]Howard Hughes Medical Institute, MIT, Cambridge, Massachusetts, USA. [4]Ben May Department for Cancer Research, The University of Chicago, Chicago, Illinois, USA. [5]Shanghai Institute of Materia Medica, Chinese Academy of Sciences, Shanghai, China. [6]Whitehead Institute for Biomedical Research, Cambridge, Massachusetts, USA. [7]Department of Anatomy and Cell Biology, University of Florida, Gainesville, Florida, USA. [8]Present address: Model Animal Research Center, Ministry of Education Key Laboratory of Model Animal for Disease Study, Nanjing University, Nanjing, China. [9]These authors contributed equally to this work. Correspondence should be addressed to L.-H.T. (lhtsai@mit.edu).

Received 3 April; accepted 11 June; published online 14 July 2013; corrected online 26 July 2013 (details online); doi:10.1038/nn.3460

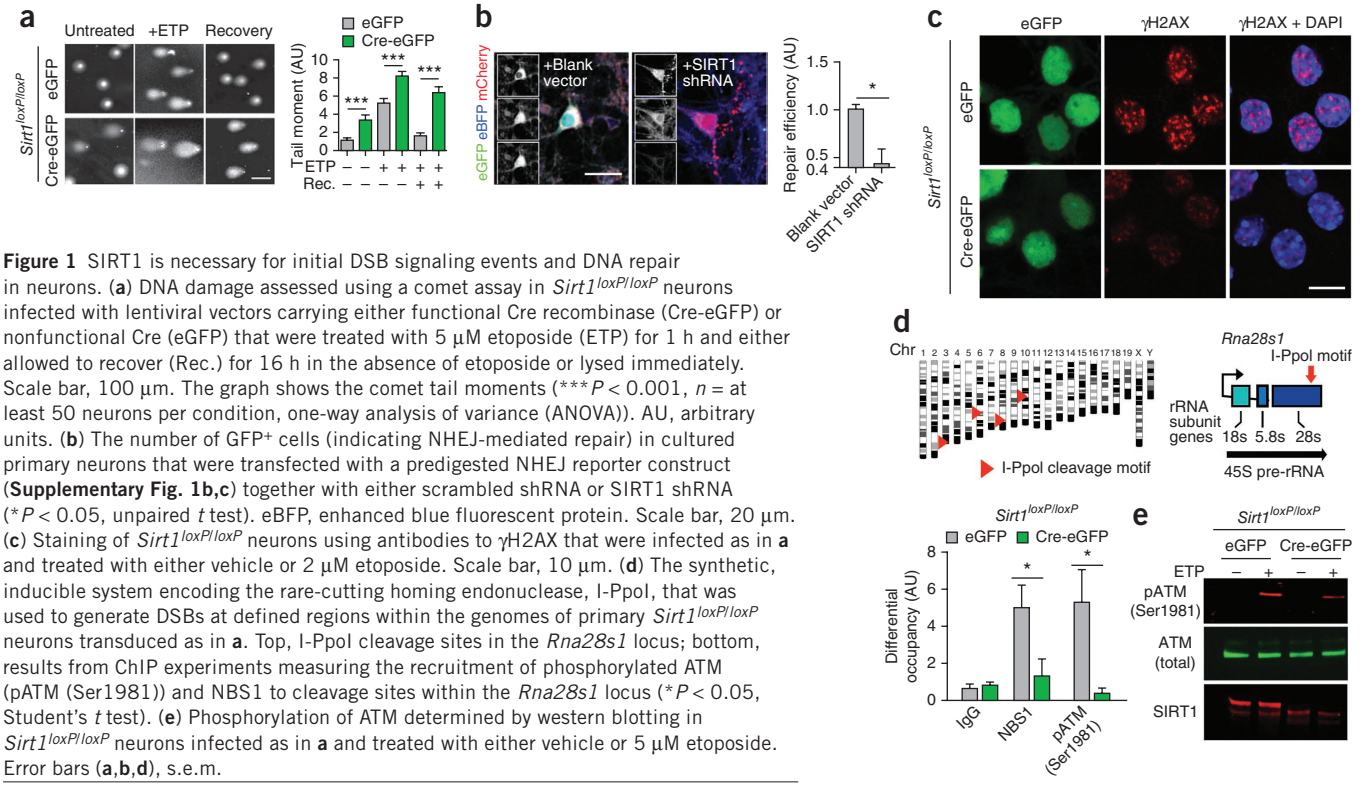

Figure 1 SIRT1 is necessary for initial DSB signaling events and DNA repair in neurons. (**a**) DNA damage assessed using a comet assay in *Sirt1*$^{loxP/loxP}$ neurons infected with lentiviral vectors carrying either functional Cre recombinase (Cre-eGFP) or nonfunctional Cre (eGFP) that were treated with 5 μM etoposide (ETP) for 1 h and either allowed to recover (Rec.) for 16 h in the absence of etoposide or lysed immediately. Scale bar, 100 μm. The graph shows the comet tail moments (***$P < 0.001$, n = at least 50 neurons per condition, one-way analysis of variance (ANOVA)). AU, arbitrary units. (**b**) The number of GFP$^+$ cells (indicating NHEJ-mediated repair) in cultured primary neurons that were transfected with a predigested NHEJ reporter construct (**Supplementary Fig. 1b,c**) together with either scrambled shRNA or SIRT1 shRNA (*$P < 0.05$, unpaired t test). eBFP, enhanced blue fluorescent protein. Scale bar, 20 μm. (**c**) Staining of *Sirt1*$^{loxP/loxP}$ neurons using antibodies to γH2AX that were infected as in **a** and treated with either vehicle or 2 μM etoposide. Scale bar, 10 μm. (**d**) The synthetic, inducible system encoding the rare-cutting homing endonuclease, I-PpoI, that was used to generate DSBs at defined regions within the genomes of primary *Sirt1*$^{loxP/loxP}$ neurons transduced as in **a**. Top, I-PpoI cleavage sites in the *Rna28s1* locus; bottom, results from ChIP experiments measuring the recruitment of phosphorylated ATM (pATM (Ser1981)) and NBS1 to cleavage sites within the *Rna28s1* locus (*$P < 0.05$, Student's t test). (**e**) Phosphorylation of ATM determined by western blotting in *Sirt1*$^{loxP/loxP}$ neurons infected as in **a** and treated with either vehicle or 5 μM etoposide. Error bars (**a**,**b**,**d**), s.e.m.

Notably, despite the elevated amounts of DNA damage (**Fig. 1a**), phosphorylation of H2AX (γH2AX) was reduced (by at least 30%) in *Sirt1* knockout neurons that were challenged with etoposide (**Fig. 1c**). We obtained similar results in neurons pretreated with the SIRT1 inhibitor sirtinol (**Supplementary Fig. 1d**), and together these findings suggest that initial events in DSB signaling could be disrupted in the absence of SIRT1 activity. To address this possibility, we first used the rare-cutting homing endonuclease I-PpoI to generate DSBs at defined loci within the genomes of cultured primary neurons[13,14]. Chromatin immunoprecipitation (ChIP) after I-PpoI induction revealed that the occupancy of phosphorylated ATM and NBS1, key DSB sensors and transducers, is attenuated at chromatin proximal to I-PpoI–generated DSBs in *Sirt1* knockout neurons (**Fig. 1d**). ATM is rapidly activated through autophosphorylation after DSB induction and in turn coordinates signaling events at DSBs through phosphorylation of its numerous targets, including H2AX[15]. In addition to being deficient in ATM recruitment, the amounts of phosphorylated ATM were also markedly reduced in etoposide-treated *Sirt1* knockout neurons compared to controls (**Fig. 1e**), indicating that SIRT1 is also essential for ATM activity. Taken together these results suggest that SIRT1 is an apical component of the neuronal DSB response whose activity is crucial for the initial sensing and signaling from DSBs and their eventual repair through NHEJ.

SIRT1 interacts physically with HDAC1

We previously showed that overexpression of the class I histone deacetylase, HDAC1, could also suppress neuronal loss during p25 expression[10]. Because both SIRT1 and HDAC1 were able to suppress neuronal loss in the same mouse model, we reasoned that the two proteins might work collaboratively to promote genomic stability in neurons. Incubation of purified recombinant Flag-tagged HDAC1 (HDAC1-Flag) with recombinant histidine-tagged SIRT1 (SIRT1-His) followed by the precipitation of HDAC1 with anti Flag–conjugated agarose beads coprecipitated SIRT1, suggesting a direct physical interaction between SIRT1 and HDAC1 (**Fig. 2a**). Notably, HDAC2, which shares ~85% similarity with HDAC1, was unable to bind SIRT1 under the same conditions (**Fig. 2a**). Next we generated and expressed multiple Flag-tagged fragments of HDAC1 (**Fig. 2b**) and mapped the interaction to the N-terminal domain (NTD) of HDAC1 (**Fig. 2c**). Notably, immunoprecipitation of endogenous HDAC1 indicated only weak binding with endogenous SIRT1 (**Fig. 2d**), but this interaction was considerably strengthened by induction of DNA damage (**Fig. 2d**).

Because an interaction between SIRT1 and HDAC1 is stimulated by DNA damage, we inquired whether SIRT1 and HDAC1 localize to sites of DNA DSBs in neurons. Colocalization analysis of cultured primary neurons revealed that SIRT1 and HDAC1 show a punctate distribution pattern that is devoid of chromocenters (subnuclear compartments consisting of densely packed chromatin) and nucleoli in mouse primary neurons. After treatment with etoposide, a substantial fraction of SIRT1 and HDAC1 colocalized with γH2AX foci (**Fig. 2e**), suggesting that both SIRT1 and HDAC1 are present at sites of DSBs in neurons. We next used laser microirradiation to generate subnuclear DSBs within the nuclei of individual Hoechst-stained primary neurons (**Supplementary Fig. 2a,b**). After microirradiation, both SIRT1 and HDAC1 showed strong enrichment within lesioned regions that were marked with γH2AX (**Fig. 2f**). In addition, we again used the I-PpoI system and targeted a unique I-PpoI cleavage site within the *Dnahc7b* locus on chromosome 1 for ChIP analysis. As described above (**Fig. 1d**), we detected a strong enrichment in phosphorylated ATM at chromatin proximal to the I-PpoI cleavage site after I-PpoI induction (**Fig. 2g**). The amounts of SIRT1 and HDAC1 were also enriched at damage-proximal chromatin after DSB generation, with pATM, SIRT1 and HDAC1 showing the strongest accumulation immediately 3′ to the cleavage site (**Fig. 2g**). Together these results suggest that SIRT1 and HDAC1 are recruited to sites of DNA DSBs in neurons.

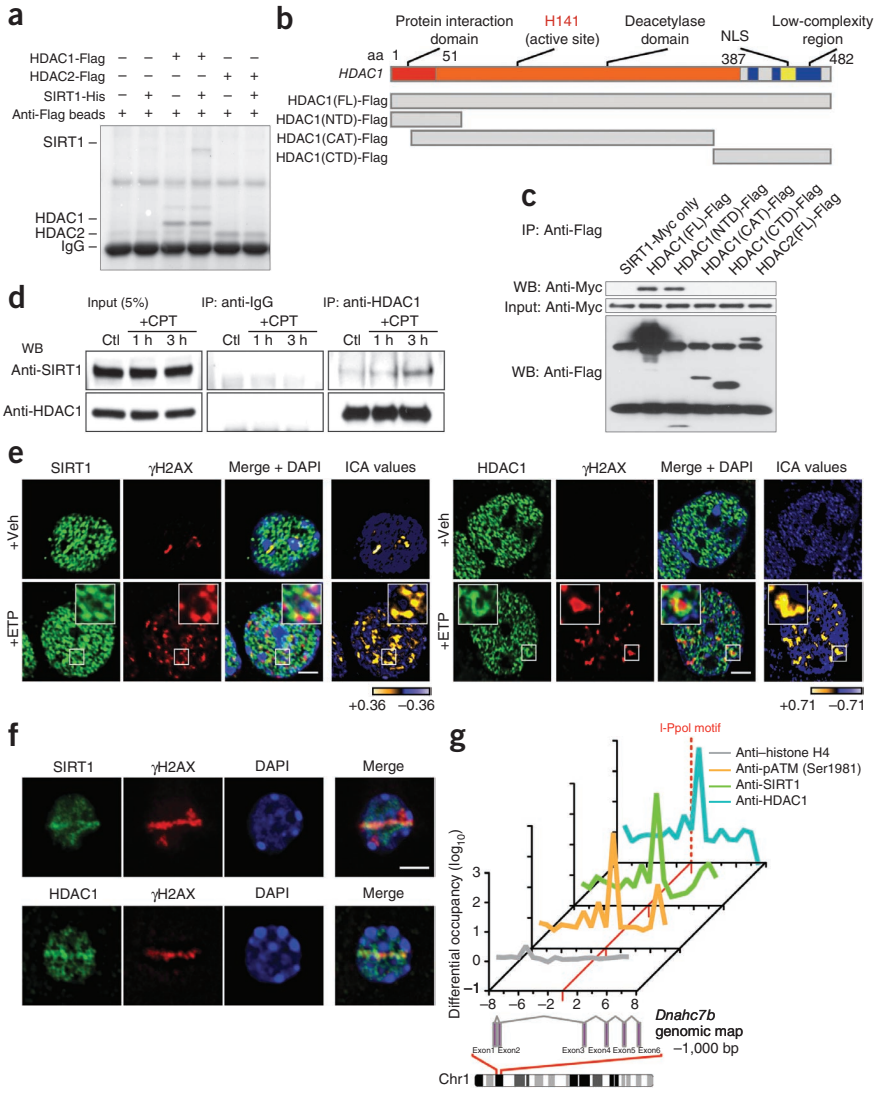

Figure 2 SIRT1 and HDAC1 interact physically and localize to DSB sites in neurons. (**a**) The ability to retain SIRT1 in recombinant SIRT1-His that was incubated with either HDAC1-Flag or HDAC2-Flag, after which HDAC1 and HDAC2 were precipitated with anti Flag–conjugated agarose beads. (**b**) Diagram illustrating HDAC1 fragment constructs for interaction mapping. FL, full length; CTD, C-terminal domain; CAT, catalytic domain; aa, amino acid. (**c**) Immunoprecipitation and blotting with antibodies to Myc of the indicated Flag-tagged fragments expressed together with SIRT1-Myc. IP, immunoprecipitation; WB, western blotting. (**d**) Blotting with antibodies to SIRT of HT22 cells that were treated with camptothecin (CPT; 1 μM) and precipitated with antibodies to HDAC1. Ctl, control (before treatment with camptothecin). (**e**) Staining of etoposide-treated primary neurons with antibodies to either SIRT1 or HDAC1 and antibodies to γH2AX. Right, an intensity correlation analysis (ICA). Pixels from the input channel covarying positively with the corresponding signal from the γH2AX channel are indicated in yellow, and pixels covarying negatively are indicated in blue. Scale bars, 3 μm; insets, ×4 magnification. Veh, vehicle; DAPI, 4′,6-diamidino-2-phenylindole. (**f**) Staining of primary neurons that were subjected to subnuclear, laser-generated DNA lesioning with antibodies to either SIRT1 or HDAC1 and antibodies to γH2AX. Scale bar, 3 μm. (**g**) Recruitment of the indicated proteins at a unique cleavage site between exons 2 and 3 in *Dnahc7b* assessed by ChIP after the rare-cutting homing endonuclease I-PpoI was used to generate DNA DSBs at defined genetic loci in mouse cortical neurons. Primers were designed at regular 1-kb intervals spanning 10 kb both 3′ and 5′ to the I-PpoI consensus site (red dashed line). Chr1, chromosome 1.

To further investigate the dynamics of SIRT1 and HDAC1 recruitment to DSB sites, we microirradiated Hoechst-stained primary neurons expressing either EmGFP-SIRT1 or HDAC1-EmGFP and monitored their localization to sites of laser-induced DSBs as a function of time. We detected an increase in EmGFP-SIRT1 accumulation in laser-lesioned regions almost immediately after DSB induction ($\tau_{1/2}$ = 3.21 ± 0.48 s (mean ± s.e.m.)) (**Fig. 3a–c**), whereas HDAC1-EmGFP accumulation became apparent by ~60 s ($\tau_{1/2}$ = 57.7 ± 5.8 s), indicating that SIRT1 localizes to DSB sites with faster kinetics than HDAC1. Next we individually knocked down various known DSB sensors and assessed their effects on SIRT1 and HDAC1 dynamics at laser-induced DSBs in live postmitotic neurons. The recruitment of SIRT1 to DSBs was strictly ATM dependent, and knockdown of ATM caused a marked reduction in both the maximal intensity and the kinetics of SIRT1 accrual at DSBs (**Fig. 3d** and **Supplementary Fig. 2c**). Thus, SIRT1 and ATM have a mutually dependent relationship, with SIRT1 being essential for ATM stability at DSBs and ATM activity after DSB induction (**Fig. 1d,e**) and ATM being necessary to recruit SIRT1 to DSBs. Conversely, the accumulation of HDAC1 was most severely affected by the knockdown of NBS1 and KU70 and KU80 (KU70/80) (**Fig. 3d**), with the latter also causing HDAC1 to accrue with slower kinetics (**Supplementary Fig. 2c**). Moreover, HDAC1 is probably recruited as part of the nucleosome remodeling and deacetylase (NuRD) complex, as knockdown of CHD4, an integral component of the NuRD complex, also severely disrupted HDAC1 localization to DSBs (**Fig. 3d**)[16]. Knockdown of individual DSB sensors had no effect on the expression of either EmGFP-SIRT1 or HDAC1-EmGFP (**Supplementary Fig. 2d**).

Overall, distinct proteins seemed to govern SIRT1 and HDAC1 recruitment to DSBs. However, because an interaction between SIRT1 and HDAC1 is enhanced by DNA damage and SIRT1 localizes to DSBs with faster kinetics than HDAC1, we tested the effect of SIRT1 knockdown on HDAC1 localization to laser-generated DSBs. In neurons transfected with SIRT1 short interfering RNAs (siRNAs), HDAC1 localization to laser-induced DSBs was markedly reduced (**Fig. 3e**), suggesting that in addition to the above factors, SIRT1 is also essential for HDAC1 recruitment. In corroboration with this finding, HDAC1 enrichment at I-PpoI–generated DSBs was also significantly diminished in *Sirt1* knockout neurons (**Fig. 3f**). Together these experiments describe the dynamics of SIRT1 and HDAC1 in response to DSB formation in living neurons, unveil a new synergistic relationship between SIRT1 and ATM that is crucial for signaling at DSBs and identify a new interaction between SIRT1 and HDAC1 that helps recruit HDAC1 to DSBs.

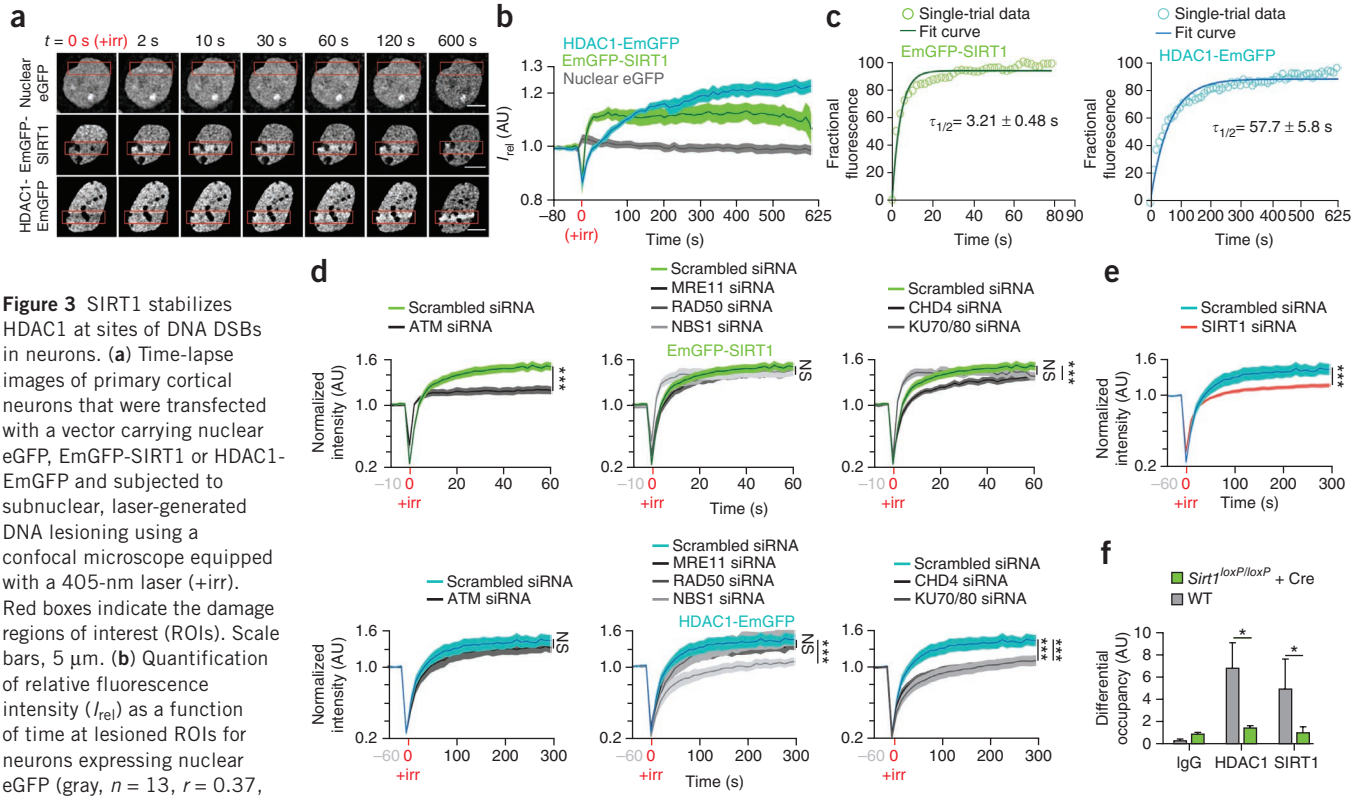

Figure 3 SIRT1 stabilizes HDAC1 at sites of DNA DSBs in neurons. (**a**) Time-lapse images of primary cortical neurons that were transfected with a vector carrying nuclear eGFP, EmGFP-SIRT1 or HDAC1-EmGFP and subjected to subnuclear, laser-generated DNA lesioning using a confocal microscope equipped with a 405-nm laser (+irr). Red boxes indicate the damage regions of interest (ROIs). Scale bars, 5 µm. (**b**) Quantification of relative fluorescence intensity (I_{rel}) as a function of time at lesioned ROIs for neurons expressing nuclear eGFP (gray, $n = 13$, $r = 0.37$, Pearson correlation), HDAC1-EmGFP (blue, $n = 15$, $r = 0.98$, Pearson correlation) or EmGFP-SIRT1 (green, $n = 11$, $r = 0.77$, Pearson correlation). (**c**) Modeling and regression analysis of the time-lapse data. Empty circles (green, SIRT1; blue, HDAC1) indicate data from a single trial plotted against the fitted curve (solid lines). The $\tau_{1/2}$ values are shown as the mean ± s.e.m. (**d**) Relative fluorescence intensity (I_{rel}) as a function of time at lesioned ROIs for neurons expressing either EmGFP-SIRT1 (top) or HDAC1-EmGFP (bottom) together with the indicated siRNAs (***$P < 0.001$, n = at least 10 measurements per condition, one-way ANOVA; the scrambled siRNA traces are reproduced in each graph for SIRT1 and HDAC1 for convenience of visualization). NS, not significant ($P > 0.05$). KU70/80 siRNA, siRNA to KU70 and KU80. (**e**) Quantification of relative fluorescence intensity (I_{rel}) as a function of time at lesioned ROIs for neurons expressing HDAC1-EmGFP together with either scrambled siRNA or SIRT1 siRNA (***$P < 0.001$, n = at least 10 independent measurements per condition, unpaired t test). (**f**) The recruitment of the indicated proteins to cleavage sites within the *Rna28s1* locus assessed using ChIP (as in **Fig. 1d**) after DSBs were generated using the I-PpoI–estrogen receptor (ER) system in wild-type (WT) and *Sirt1* knockout primary neurons (*$P < 0.05$, $n = 3$, unpaired t test). Error bars (**b**,**d**–**f**), s.e.m.

SIRT1 deacetylates HDAC1 and stimulates its enzymatic activity

Although an important function of the physical interaction between SIRT1 and HDAC1 could be to facilitate the recruitment of HDAC1 to DSB sites (**Fig. 3e**,**f**), HDAC1 is acetylated by the p300 acetyltransferase, and acetylation of HDAC1 inhibits its deacetylase activity[17]. We therefore posited that the interaction of SIRT1 with HDAC1 might lead to the deacetylation and activation of HDAC1. Incubation of recombinant HDAC1 with increasing amounts of p300 recapitulated the previous observation that p300 acetylates HDAC1 (**Supplementary Fig. 3a**)[17], whereas titration of SIRT1 in the HDAC1-p300 reactions decreased the acetylation of HDAC1 in a dose-dependent manner (**Fig. 4a**). In addition, whereas overexpression of HDAC1 together with p300 resulted in increased HDAC1 acetylation, coexpression of SIRT1 caused marked HDAC1 deacetylation (**Fig. 4b**), suggesting that SIRT1 can deacetylate HDAC1.

We next determined whether SIRT1-mediated deacetylation of HDAC1 affects its enzymatic activity. In a fluorescence-based reporter assay (**Supplementary Fig. 3b**), incubation of recombinant HDAC1 with p300 caused an approximate 40% reduction in HDAC1 activity, whereas its activity was stimulated by about 30% in the presence of SIRT1 (**Fig. 4c**). In addition, immunoprecipitated HDAC1 from *Sirt1* knockout neurons showed a significant deficit in enzymatic activity compared to HDAC1 precipitated from control neurons (**Fig. 4d**). Conversely, SIRT1 overexpression resulted in stimulation of HDAC1 activity (**Supplementary Fig. 3c**). Together these results suggest that SIRT1-mediated deacetylation of HDAC1 stimulates its activity.

To specifically determine the residues within HDAC1 that are deacetylated by SIRT1, we incubated recombinant HDAC1 with either p300 alone or p300 and SIRT1 as described above and subjected the reaction mixtures to analysis by mass spectrometry. In the presence of p300 alone, HDAC1 was readily acetylated at residues Lys89, Lys220, Lys412, Lys432, Lys438, Lys439 and Lys441 (**Fig. 4e**–**g**). Label-free quantification indicated that the addition of SIRT1 resulted in decreased acetylation at all sites except Lys412 (**Fig. 4g**). Moreover, we did not detect acetylation at two of these residues, Lys220 and Lys432, using the mass spectrometry assay, suggesting substantial deacetylation activity of SIRT1 on the two acetyl-lysine residues (**Fig. 4g**). An antibody that specifically recognizes acetylated Lys432 of HDAC1 (ref. 18) and quantitative western blotting further confirmed the ability of SIRT1 to deacetylate HDAC1 at this residue (**Fig. 4h**). Similarly, treatment of HEK293T cells with a pharmacological SIRT1 activator (compound #10)[19] decreased HDAC1 acetylation at Lys432 in a dose-dependent manner (**Fig. 4i**). Furthermore, in a computationally predicted tertiary structure of HDAC1 (**Supplementary Fig. 3d**), the proximity of the region containing Lys432 to the NTD indicates that the binding of SIRT1 at the NTD could allow for deacetylation of residues at the C terminus.

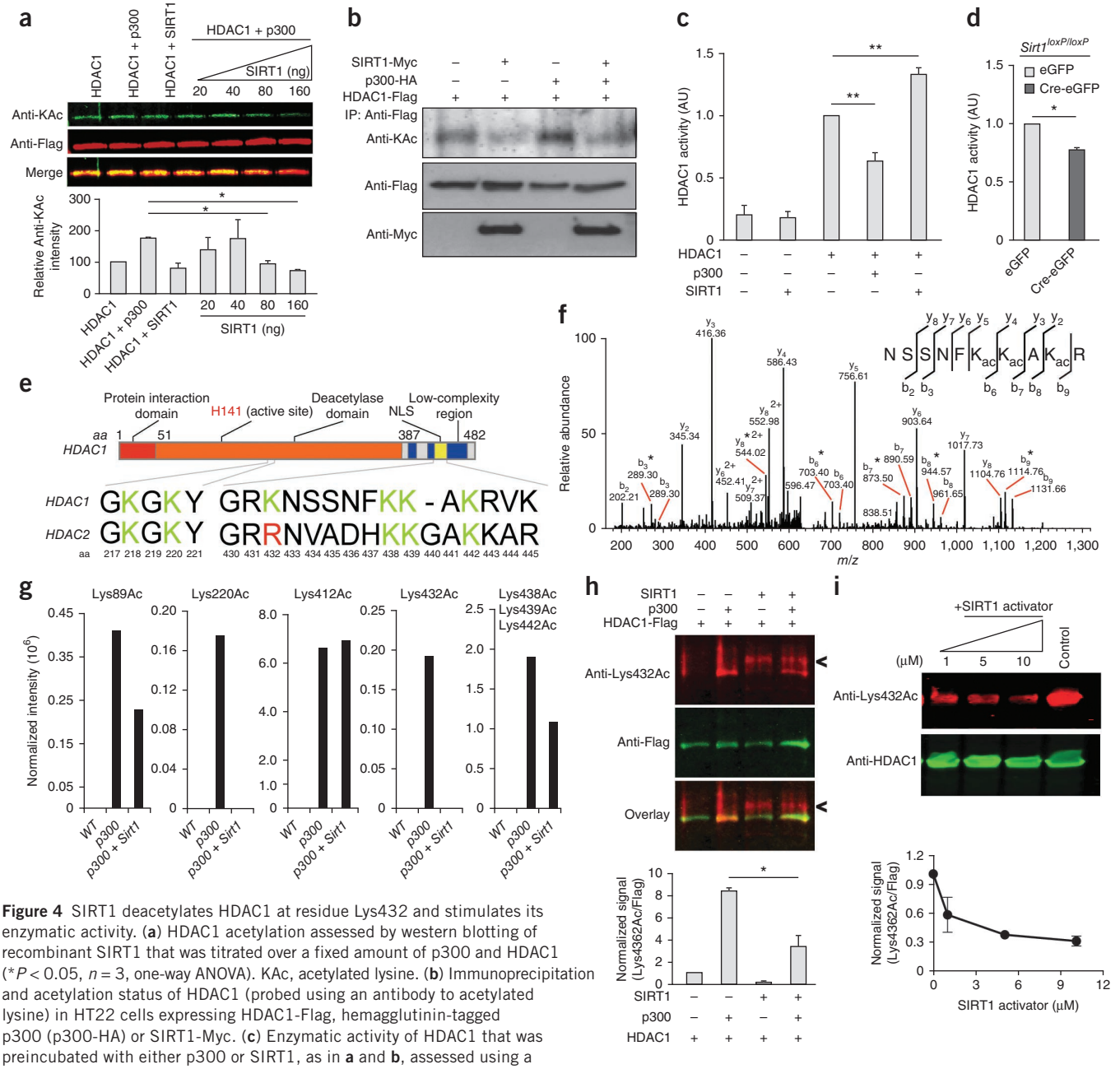

Figure 4 SIRT1 deacetylates HDAC1 at residue Lys432 and stimulates its enzymatic activity. (**a**) HDAC1 acetylation assessed by western blotting of recombinant SIRT1 that was titrated over a fixed amount of p300 and HDAC1 (*$P < 0.05$, $n = 3$, one-way ANOVA). KAc, acetylated lysine. (**b**) Immunoprecipitation and acetylation status of HDAC1 (probed using an antibody to acetylated lysine) in HT22 cells expressing HDAC1-Flag, hemagglutinin-tagged p300 (p300-HA) or SIRT1-Myc. (**c**) Enzymatic activity of HDAC1 that was preincubated with either p300 or SIRT1, as in **a** and **b**, assessed using a fluorescence-based HDAC enzymatic activity assay (**Supplementary Fig. 3b**) (**$P < 0.01$, $n = 3$, one-way ANOVA). (**d**) Immunoprecipitation and enzymatic activity of HDAC1, as in **c**, in *Sirt1*$^{loxP/loxP}$ neurons that were infected with Cre-eGFP and eGFP lentiviral vectors (*$P < 0.05$, $n = 3$, unpaired *t* test). (**e**) Diagram depicting the acetylated lysine residues in HDAC1 and HDAC2. (**f**) Annotated tandem mass spectrometry spectrum of the lysine-acetylated peptide NSSNFK$_{ac}$K$_{ac}$AK$_{ac}$R (where subscript ac denotes acetylation) that identified lysine acetylation sites at Lys438, Lys439 and Lys441 of HDAC1 after reaction with p300. The b and y ions represent collision-induced peptide fragment ions containing the N or C terminal, respectively. The asterisks indicate fragment ions with neutral loss of amine. (**g**) Label-free quantification for each lysine acetylation site using a protein abundance–normalized peptide-precursor ion intensity showing that lysine acetylation abundance on p300-treated HDAC1 decreased after the addition of SIRT1 to the reaction. Ac, acetylation of the indicated lysine. (**h**) Acetylation of HDAC1, as in **a**, of recombinant SIRT1 that was incubated together with p300 and HDAC1 assessed using an antibody specific to acetylated Lys432. The arrowheads indicate nonspecific cross-reacting bands in the lanes containing recombinant SIRT1 (*$P < 0.05$, $n = 3$, unpaired *t* test). (**i**) HDAC1 acetylation at Lys432 in HEK293T cells that were treated with the indicated concentrations of the SIRT1 activator compound #10 for 12 h. Error bars (**a**,**c**,**d**,**h**,**i**), s.e.m.

Of all the acetylatable residues in HDAC1, Lys432 has been shown to be particularly important for its enzymatic activity, and mutation of this residue to an acetyl-mimetic glutamine (K432Q) almost completely abolished HDAC1 activity[17]. Moreover, whereas the remaining lysines are conserved between HDAC1 and the closely related HDAC2, Lys432 in HDAC1 is occupied instead by arginine in HDAC2 (**Fig. 4e**), and HDAC1, but not HDAC2, can be acetylated by p300 (refs. 17,20). Taken together these results suggest that in addition to facilitating the recruitment of HDAC1 to DSB sites, SIRT1 also exists in an enzyme-substrate relationship with HDAC1 wherein SIRT1 deacetylates HDAC1 at a crucial lysine residue, Lys432, thereby stimulating its enzymatic activity.

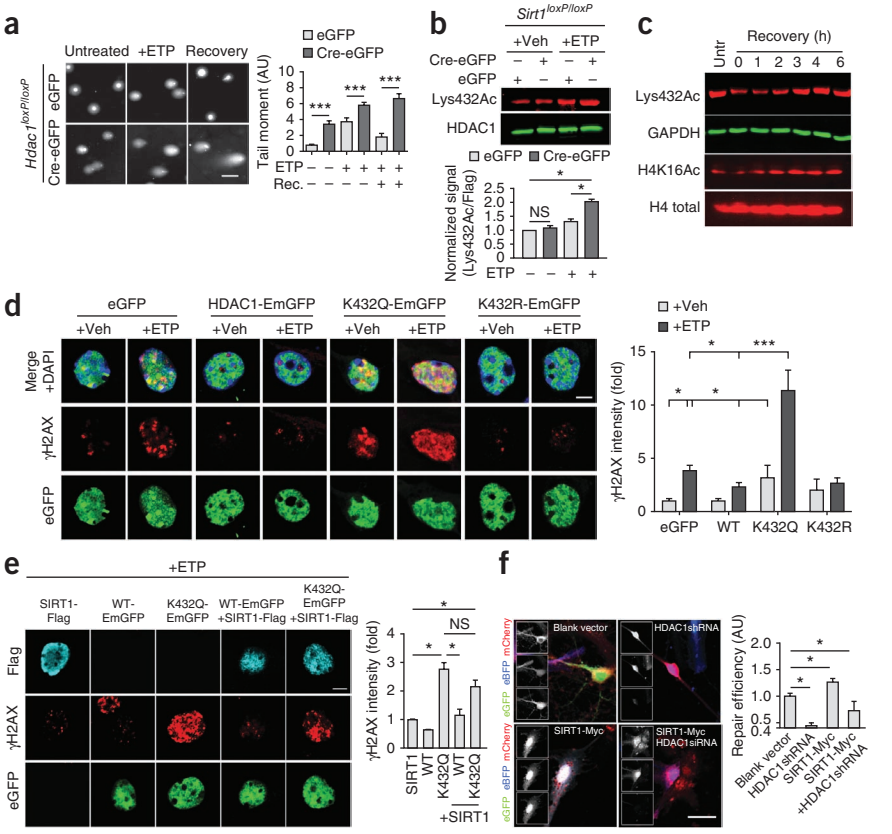

Figure 5 Deacetylation of HDAC1 is essential for DSB repair in neurons. (**a**) DNA damage assessed using the comet assay in *Hdac1*$^{loxP/loxP}$ neurons that were infected as in **Figure 1a** and treated with etoposide (***$P < 0.001$, n = at least 50 neurons per condition, one-way ANOVA). Scale bar, 100 μm. (**b**) HDAC acetylation at Lys432 assessed by western blotting of primary neurons cultured from *Sirt1*$^{loxP/loxP}$ embryos that were infected as in **Figure 1a** and treated with 5 μM etoposide for 2 h (*$P < 0.05$, $n = 3$ independent experiments, one-way ANOVA). (**c**) Western blot analysis probing the indicated acetylation marks in cultured primary neurons (7 d *in vitro*) that were treated with 5 μM etoposide for 30 min, after which the cells were lysed either immediately or after recovery from etoposide washout for the indicated times and electrophoresed. Untr, untreated. (**d**) Staining with antibodies to γH2AX of primary neurons that were transfected with the indicated vectors and treated with etoposide (2 μM) for 1 h. Scale bar, 10 μm (*$P < 0.05$, ***$P < 0.001$, n = at least 25 neurons per condition and 4 independent experiments, one-way ANOVA). (**e**) As in **d** but using cultured primary neurons expressing SIRT1-Flag together with either HDAC1-EmGFP or HDAC1^{K432Q}-EmGFP that were treated with etoposide (2 μM) for 1 h. Scale bar, 15 μm. The quantification is shown to the right (*$P < 0.05$, n = at least 25 neurons per condition and 3 independent experiments, one-way ANOVA). (**f**) The number of GFP$^+$ cells (assessed as a measure of DNA repair using NHEJ) of cultured primary neurons expressing either SIRT1 together with HDAC1 shRNA that were transfected with the predigested NHEJ reporter construct (*$P < 0.05$, $n = 3$ independent experiments, one-way ANOVA). Error bars (**a**,**b**,**d**–**f**), s.e.m.

HDAC1 deacetylation by SIRT1

To understand whether HDAC1 deacetylation has a role in DSB signaling and repair in neurons, we characterized the effects of HDAC1 loss in these processes. In comet assays, *Hdac1* knockout neurons had longer tail moments than controls and, similarly to *Sirt1* knockout neurons (**Fig. 1a**), were unable to recover from etoposide-induced DSBs (**Fig. 5a**). This suggests that neurons become more susceptible to DSBs in the absence of HDAC1 and that HDAC1 is essential for DSB repair in neurons. In contrast to SIRT1, however, HDAC1 had no effect on ATM autophosphorylation (**Supplementary Fig. 4a**), and γH2AX intensity was increased in *Hdac1* knockout neurons compared to controls after etoposide treatment (**Supplementary Fig. 4b**). We obtained similar results in cultured primary neurons expressing a catalytically inactive HDAC1, HDAC1^{H141Y} (**Supplementary Fig. 4c**). Thus, although HDAC1 is essential for DNA repair in neurons, initial events in DSB signaling such as ATM and H2AX phosphorylation do not require HDAC1 activity. These results are consistent with the notion that HDAC1 functions downstream of SIRT1 in the DSB response.

We next assessed the status of HDAC1 acetylation in *Sirt1* knockout neurons after etoposide treatment. Whereas HDAC1 acetylation at Lys432 was increased in etoposide-treated control neurons, this increase was far more pronounced in *Sirt1* knockout neurons (**Fig. 5b**), suggesting that the acetylation of HDAC1 is modulated in response to DSB formation and that SIRT1 maintains HDAC1 in a deacetylated and active state in neurons. However, given that HDAC1 is essential for DSB repair, we found it peculiar that the acetylation of HDAC1 is elevated after DSB formation. To further clarify this matter, we briefly treated cultured primary neurons with etoposide (30 min) followed by washout and recovery in etoposide-free medium. We then prepared lysates at hourly intervals and monitored HDAC1 acetylation at Lys432 as a function of time after etoposide treatment. Notably, compared to untreated controls, neurons treated with etoposide for 30 min showed a reduction in Lys432 acetylation (**Fig. 5c**). This trend continued until 1 h after etoposide washout, after which time the amount of acetylated Lys432 began to rise again, surpassing the amount of acetylation in untreated controls by about 4 h after washout (**Fig. 5c**). Furthermore, this pattern of HDAC1 acetylation mirrored changes in the acetylation of histone H4 Lys16 (H4K16) (**Fig. 5c**), a previously identified HDAC1 target[21], and the amount of H4K16 acetylation was increased in *Hdac1* knockout neurons (**Supplementary Fig. 4d**).

To further understand the importance of HDAC1 deacetylation in the DSB response, we overexpressed eGFP-tagged variants of HDAC1 carrying either a K432Q (acetylation mimetic) or a K432R (acetylation resistant) mutation in cultured primary neurons. In control neurons expressing eGFP alone, etoposide treatment readily triggered the formation of γH2AX foci, and consistent with previous observations, overexpression of HDAC1-EmGFP caused a reduction in the number of γH2AX foci (**Fig. 5d**). In contrast, neurons expressing the K432Q mutant showed γH2AX foci even in the absence of etoposide treatment and a substantial increase in the number of foci in the presence of etoposide (**Fig. 5d**). Conversely, neurons expressing the K432R mutant had a modest reduction in γH2AX intensity compared to controls, indicating that constitutive acetylation of HDAC1 renders neurons more susceptible to genotoxic insults, especially DSBs.

Because SIRT1 stimulates HDAC1 through deacetylation, we predicted that the acetyl-mimetic HDAC1^{K432Q} mutant would also be refractory to the effects of SIRT1 overexpression. In the presence of etoposide, neurons overexpressing SIRT1 showed a significant

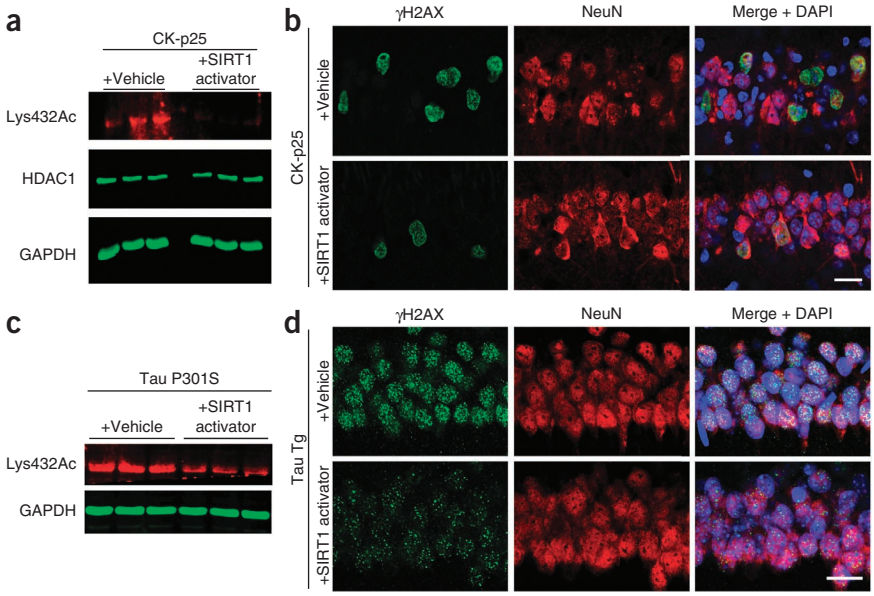

Figure 6 Pharmacological SIRT1 activation can protect neurons against DNA damage *in vivo*. (**a**) Acetylation of HDAC1 at Lys432 assessed by quantitative western blotting in brain lysates of CK-p25 mice that expressed the p25 transgene for 6 weeks and were administered either vehicle or 30 mg per kg body weight of compound #10. (**b**) Representative immunohistochemical images showing γH2AX and NeuN staining in CK-p25 mice that expressed the p25 transgene for 6 weeks and were administered either compound #10 or vehicle (Online Methods). Scale bar, 100 μm. (**c**) HDAC1 acetylation at Lys432 assessed by western blotting of hippocampal lysates from 2-month old tau P301S transgenic mice that were treated with SIRT1 activator (**d**) Brain sections from 2-month-old P301S transgenic (Tg) mice that were administered either vehicle or 30 mg per kg body weight of compound #10 through oral gavage (5 mice per group) once daily for 2 weeks stained with antibodies to γH2AX and NeuN. Scale bar, 100 μm.

reduction in the number of γH2AX foci compared to controls (data not shown); however, SIRT1 overexpression had little effect on γH2AX intensity in neurons also expressing the HDAC1^{K432Q} mutant (**Fig. 5e**). Similarly to SIRT1 overexpression, treatment of neurons with the pharmacological SIRT1 activator also caused a reduction in γH2AX intensity (**Supplementary Fig. 4e**,**f**), and neurons expressing the K432Q and K432R mutants were also refractory to a SIRT1 activator–mediated reduction in γH2AX intensity (**Supplementary Fig. 4f**). Mutation of the lysine residue to glutamine had no effect on the ability of HDAC1 to bind SIRT1 (**Supplementary Fig. 4g**). However, expression of the NTD fragment of HDAC1, which would compete with endogenous HDAC1 for SIRT1 binding, resulted in increased γH2AX intensity compared to controls (**Supplementary Fig. 4f**). Also, SIRT1 activator treatment could not stimulate the activity of purified recombinant HDAC1 directly in the absence of SIRT1 (**Supplementary Fig. 4g**). We again used the fluorescence-based NHEJ reporter system wherein we transfected the predigested reporter construct in neurons expressing SIRT1 together with either a control short hairpin RNA (shRNA) or HDAC1 shRNA. SIRT1 overexpression in neurons stimulated NHEJ-mediated DSB repair, as indicated by an increase in GFP$^+$ cells compared controls (**Fig. 5f**). However, this increase was attenuated in neurons expressing HDAC1 shRNA (**Fig. 5f**). Taken together these results suggest that the ability of SIRT1 to protect against DNA damage and stimulate DNA repair requires it to interact with and deacetylate HDAC1.

On the basis of these observations, we assessed whether SIRT1 activation also affects the number of DSBs and HDAC1 acetylation in neurodegenerating CK-p25 mice by orally administering the pharmacological SIRT1 activator to these mice. Western blot analysis of hippocampal lysates after 6 weeks of p25 induction revealed a sharp reduction in HDAC1 Lys432 acetylation in the CK-p25 mice that we treated with the SIRT1 activator compared to CK-p25 mice treated with a vehicle control (**Fig. 6a**). In addition, whereas vehicle-treated CK-p25 mice had a marked increase in the number of γH2AX-positive cells in the hippocampus, the number of γH2AX-positive cells was reduced by about 40% in CK-p25 mice administered the SIRT1 activator (**Fig. 6b**). These results suggest a strong correlation between SIRT1 activation, HDAC1 deacetylation and a reduction in the number of DNA DSBs. Additionally, administration of the SIRT1 activator was also able to reduce HDAC1 acetylation and γH2AX intensity in 2-month-old human tau transgenic (P301S) mice[22] (**Fig. 6c**,**d**). Together these results highlight the therapeutic potential of SIRT1 activators against neurodegeneration.

DISCUSSION

Overall our data suggest that SIRT1 primes the cellular response to DNA DSBs by stimulating the activities of ATM and HDAC1. After being recruited to DSBs in an ATM-dependent manner, SIRT1 in turn stimulates ATM autophosphorylation and ATM recruitment to DSB sites and thereby primes the cellular DSB signaling cascade (**Supplementary Fig. 5**). After DSB induction, the MRE11-RAD50-NBS1 complex is known to activate ATM through an interaction between NBS1 and ATM[23]. SIRT1 also interacts with and deacetylates NBS1 (ref. 24), and NBS1 recruitment to DSBs is compromised in *Sirt1* knockout neurons (**Fig. 1d**). It is therefore intriguing to consider the SIRT1-NBS1 interaction as a potential mechanism of ATM activation. However, ATM is also known to be an acetylated protein[25], and an equally interesting possibility involves SIRT1-mediated deacetylation of ATM being important for ATM autophosphorylation and activity.

In addition to activating ATM, SIRT1 participates in conjunction with KU70/80, NBS1 and the NuRD complex to stabilize HDAC1 at DSB sites. Furthermore, SIRT1 deacetylates and stimulates HDAC1, thus facilitating the dynamic regulation of HDAC1 activity that is essential for DSB repair through NHEJ. Our data are consistent with the notion that HDAC1 functions in DNA repair by affecting chromatin configuration through epigenetic modification. For instance, acetylation of H4K16 and H3K56 decrease in an HDAC1- and HDAC2-dependent manner after DSB induction, and the inability to deacetylate these residues results in more relaxed chromatin and decreased amounts of DNA repair[21,26]. However, an 'open' chromatin configuration is also important for repair because it allows repair proteins to access damaged sites easily[26]. The 'closed' chromatin configuration (probably mediated by HDAC1 and other proteins) in the initial stages after DSB formation could allow for the broken DNA ends to be retained in close proximity and for transcriptional silencing in their vicinity, after which controlled 'opening' of the chromatin could grant access to repair and signaling factors. The dynamic modulation of HDAC1 activity through its acetylation and the biphasic pattern of H4K16 acetylation (**Fig. 5c**)[21] are consistent with such a model. We demonstrate

here that one arm of such modulation is conferred by SIRT1, which deacetylates and activates HDAC1. The other arm, probably involving an acetyltransferase that inactivates HDAC1, awaits discovery. Several histone acetyltransferases (HATs), including p300, hMOF and TIP60, are known to function in the DNA DSB response[27–29]. Moreover, these HATs are also deacetylated by SIRT1, and SIRT1-mediated deacetylation has been shown to inhibit their HAT activity[30,31]. The importance of these interactions in chromatin organization and signaling at DSBs is only beginning to be unraveled, and although our work emphasizes the role of the SIRT1-HDAC1 connection in DSB repair, the relative importance of SIRT1-mediated deacetylation of the above-mentioned substrates warrants further investigation.

In neurodegenerative disorders such as Alzheimer's disease, Parkinson's disease and amyotrophic lateral sclerosis, the major risk factor is age itself[32]. Microarray analysis of postmortem human brain samples has revealed that genes encoding for synaptic transmission, learning and memory are downregulated after age 45, and this is associated with elevated amounts of oxidative damage in the promoters of the downregulated genes[1]. In addition, DNA DSBs and an upregulation of DNA damage–response genes precede the emergence of all other Alzheimer's disease–like neuropathological hallmarks in CK-p25 mice[10], and elevated amounts of DNA strand breaks have been observed in the Alzheimer's disease brain[3]. Together these results raise the possibility that the accrual of DNA damage with age could underlie the pathological changes that are associated with neurological disease. SIRT1 is known to directly modulate synaptic plasticity and memory formation[33], and SIRT1 redistribution in response to chronic DNA damage is thought to underlie some of the transcriptional changes in the aging brain[34]. Considering these observations, the benefits conferred by pharmacological activation of SIRT1 could be substantial.

METHODS

Methods and any associated references are available in the online version of the paper.

Note: Supplementary information is available in the online version of the paper.

ACKNOWLEDGMENTS

We thank F.W. Alt (Harvard Medical School) and E.N. Olson (University of Texas Southwestern Medical Center) for providing the *Sirt1*$^{loxP/loxP}$ and *Hdac1*$^{loxP/loxP}$ mice, respectively; R. Huganir (Johns Hopkins University) for providing the lentiviral Cre constructs; V. Suri, J. Ellis and G. Vlasuk (Sirtris) for providing compound #10 and, together with J. Gräff, for critical comments on the manuscript; M. Kastan (St. Jude's Medical Research Hospital) for gifting the I-PpoI-ER construct; and V. Gorbunova (University of Rochester) for providing the NHEJ constructs. This work was supported by funding from US National Institutes of Health (NIH) PO1 grant AG27916, the Howard Hughes Medical Institute, the Neurodegeneration Consortium and the Glenn award for research in biological mechanisms of aging to L.-H.T., NIH grant R01 HL095674 to Y.Q. and NIH grant U54 RR020389 to Y.Z. M.M.D. was supported by NIH training grants T32 GM007484 and T32 MH081728.

AUTHOR CONTRIBUTIONS

This study was designed by M.M.D., R.M. and L.-H.T. and was directed and coordinated by L.-H.T. M.M.D. and R.M. planned and performed most of the experiments. L.P. maintained the *Sirt1*$^{loxP/loxP}$ and *Hdac1*$^{loxP/loxP}$ mice and, together with B.A., helped with the microirradiation experiments. Y.C. and Y.Z. conducted the mass spectrometry analysis of HDAC1 acetylation. D.K. and J.G. performed some preliminary experiments with CK-p25 mice, and J.G. performed the compound #10 treatment and subsequent analysis of CK-p25 mice. P.-C.P. contributed to statistical analysis and quantification of several experiments, and Y.Q. developed and provided the antibody to acetylated HDAC1 Lys432. R.M., M.M.D. and L.-H.T. wrote the manuscript with critical input from all the authors.

COMPETING FINANCIAL INTERESTS

The authors declare no competing financial interests.

1. Lu, T. *et al.* Gene regulation and DNA damage in the ageing human brain. *Nature* **429**, 883–891 (2004).
2. Rass, U., Ahel, I. & West, S.C. Defective DNA repair and neurodegenerative disease. *Cell* **130**, 991–1004 (2007).
3. Adamec, E., Vonsattel, J.P. & Nixon, R.A. DNA strand breaks in Alzheimer's disease. *Brain Res.* **849**, 67–77 (1999).
4. Ferrante, R.J. *et al.* Evidence of increased oxidative damage in both sporadic and familial amyotrophic lateral sclerosis. *J. Neurochem.* **69**, 2064–2074 (1997).
5. Nouspikel, T. & Hanawalt, P.C. When parsimony backfires: neglecting DNA repair may doom neurons in Alzheimer's disease. *Bioessays* **25**, 168–173 (2003).
6. Gan, L. & Mucke, L. Paths of convergence: sirtuins in aging and neurodegeneration. *Neuron* **58**, 10–14 (2008).
7. Kim, D. *et al.* SIRT1 deacetylase protects against neurodegeneration in models for Alzheimer's disease and amyotrophic lateral sclerosis. *EMBO J.* **26**, 3169–3179 (2007).
8. Cruz, J.C., Tseng, H.C., Goldman, J.A., Shih, H. & Tsai, L.H. Aberrant Cdk5 activation by p25 triggers pathological events leading to neurodegeneration and neurofibrillary tangles. *Neuron* **40**, 471–483 (2003).
9. Cruz, J.C. *et al.* p25/cyclin-dependent kinase 5 induces production and intraneuronal accumulation of amyloid-β *in vivo*. *J. Neurosci.* **26**, 10536–10541 (2006).
10. Kim, D. *et al.* Deregulation of HDAC1 by p25/Cdk5 in neurotoxicity. *Neuron* **60**, 803–817 (2008).
11. Singh, N.P., McCoy, M.T., Tice, R.R. & Schneider, E.L. A simple technique for quantitation of low levels of DNA damage in individual cells. *Exp. Cell Res.* **175**, 184–191 (1988).
12. Seluanov, A., Mittelman, D., Pereira-Smith, O.M., Wilson, J.H. & Gorbunova, V. DNA end joining becomes less efficient and more error-prone during cellular senescence. *Proc. Natl. Acad. Sci. USA* **101**, 7624–7629 (2004).
13. Berkovich, E., Monnat, R.J. Jr. & Kastan, M.B. Roles of ATM and NBS1 in chromatin structure modulation and DNA double-strand break repair. *Nat. Cell Biol.* **9**, 683–690 (2007).
14. Berkovich, E., Monnat, R.J. Jr. & Kastan, M.B. Assessment of protein dynamics and DNA repair following generation of DNA double-strand breaks at defined genomic sites. *Nat. Protoc.* **3**, 915–922 (2008).
15. Shiloh, Y. ATM and related protein kinases: safeguarding genome integrity. *Nat. Rev. Cancer* **3**, 155–168 (2003).
16. Polo, S.E., Kaidi, A., Baskcomb, L., Galanty, Y. & Jackson, S.P. Regulation of DNA-damage responses and cell-cycle progression by the chromatin remodelling factor CHD4. *EMBO J.* **29**, 3130–3139 (2010).
17. Qiu, Y. *et al.* HDAC1 acetylation is linked to progressive modulation of steroid receptor-induced gene transcription. *Mol. Cell* **22**, 669–679 (2006).
18. Yang, T. *et al.* Acetylation of histone deacetylase 1 regulates NuRD corepressor complex activity. *J. Biol. Chem.* **287**, 40279–40291 (2012).
19. Dai, H. *et al.* SIRT1 activation by small molecules: kinetic and biophysical evidence for direct interaction of enzyme and activator. *J. Biol. Chem.* **285**, 32695–32703 (2010).
20. Luo, Y. *et al.* Trans-regulation of histone deacetylase activities through acetylation. *J. Biol. Chem.* **284**, 34901–34910 (2009).
21. Miller, K.M. *et al.* Human HDAC1 and HDAC2 function in the DNA-damage response to promote DNA nonhomologous end-joining. *Nat. Struct. Mol. Biol.* **17**, 1144–1151 (2010).
22. Yoshiyama, Y. *et al.* Synapse loss and microglial activation precede tangles in a P301S tauopathy mouse model. *Neuron* **53**, 337–351 (2007).
23. Lee, J.H. & Paull, T.T. Activation and regulation of ATM kinase activity in response to DNA double-strand breaks. *Oncogene* **26**, 7741–7748 (2007).
24. Yuan, Z., Zhang, X., Sengupta, N., Lane, W.S. & Seto, E. SIRT1 regulates the function of the Nijmegen breakage syndrome protein. *Mol. Cell* **27**, 149–162 (2007).
25. Sun, Y., Jiang, X., Chen, S., Fernandes, N. & Price, B.D. A role for the Tip60 histone acetyltransferase in the acetylation and activation of ATM. *Proc. Natl. Acad. Sci. USA* **102**, 13182–13187 (2005).
26. Ball, A.R. Jr. & Yokomori, K. Damage site chromatin: open or closed? *Curr. Opin. Cell Biol.* **23**, 277–283 (2011).
27. Yuan, Z.M. *et al.* Role for p300 in stabilization of p53 in the response to DNA damage. *J. Biol. Chem.* **274**, 1883–1886 (1999).
28. Ikura, T. *et al.* Involvement of the TIP60 histone acetylase complex in DNA repair and apoptosis. *Cell* **102**, 463–473 (2000).
29. Sykes, S.M. *et al.* Acetylation of the p53 DNA-binding domain regulates apoptosis induction. *Mol. Cell* **24**, 841–851 (2006).
30. Bouras, T. *et al.* SIRT1 deacetylation and repression of p300 involves lysine residues 1020/1024 within the cell cycle regulatory domain 1. *J. Biol. Chem.* **280**, 10264–10276 (2005).
31. Peng, L. *et al.* SIRT1 negatively regulates the activities, functions, and protein levels of hMOF and TIP60. *Mol. Cell. Biol.* **32**, 2823–2836 (2012).
32. Yankner, B.A., Lu, T. & Loerch, P. The aging brain. *Annu. Rev. Pathol.* **3**, 41–66 (2008).
33. Gao, J. *et al.* A novel pathway regulates memory and plasticity via SIRT1 and miR-134. *Nature* **466**, 1105–1109 (2010).
34. Oberdoerffer, P. *et al.* SIRT1 redistribution on chromatin promotes genomic stability but alters gene expression during aging. *Cell* **135**, 907–918 (2008).

ONLINE METHODS

Mouse strains, expression constructs, shRNA constructs and virus generation. All mouse work was approved by the Committee for Animal Care of the Division of Comparative Medicine at MIT. *Hdac1*$^{loxP/loxP}$ and *Sirt1*$^{loxP/loxP}$ mice were the kind gifts of E.N. Olson and F.W. Alt, respectively, and were as described[35,36]. Mouse HDAC1 and SIRT1 were subcloned into the pcDNA6.2/C-EmGFP Gateway Vector (Invitrogen, V355-20) and the pcDNA6.2/N-EmGFP Gateway Vector (Invitrogen, V356-20), resulting in C-terminal and N-terminal fusion proteins, respectively. HDAC1 fragments were constructed according to functional protein domains as determined by bioinformatic analysis with Pfam and as described previously[37]. The Stratagene QuikChange Site-Directed Mutagenesis Kit (Stratagene, 200518) was used to generate HDAC1 mutants mimicking either a constitutively acetylated or nonacetylatable state at amino acid position 432 (K432Q and K432R, respectively). Because fusion of several different affinity tags to the N terminus of HDAC1 has been shown to interfere with its catalytic activity, all HDAC1 fusion constructs were generated as C-terminal fusions. HDAC1 and SIRT1 shRNA constructs and catalytic residue mutants were as previously described[7,10]. The HA–ER–I-PpoI overexpression construct was obtained from the lab of M. Kastan (St. Jude's Children's Research Hospital)[13,14] and was modified for the production of lentivirus by subcloning into a lentiviral backbone containing T2A–red fluorescent protein (RFP) under the control of the PGK promoter. Lentiviral constructs, lenti-Cre and lenti-ΔCre, were the kind gift of R. Huganir (Johns Hopkins University) and were as reported previously[38]. Pooled siRNA oligonucleotides targeting mouse SIRT1 (sc-40987), HDAC1 (sc-29344), ATM (sc-29762), MRE11 (sc-37396), NBS1 (sc-36062) and RAD50 (sc-37398) and control scrambled siRNA (sc-37007) were obtained from Santa Cruz Biotechnologies. Pooled siRNA oligonucleotides targeting mouse KU70 (EMU067171) and KU80 (EMU053211) were obtained from Sigma-Aldrich. Pooled siRNA oligonucleotides targeting mouse Chd4 (L-052142-00-0005) were obtained from Dharmacon.

Antibodies. HDAC1 antibodies to acetylated HDAC1 (Lys432Ac) were generated from rabbits injected with an acetylated C-terminal peptide (peptide sequence GEGGRK$_{ac}$NSSNF). The antibodies used for staining were as follows: anti-HDAC1 1.T9 (Abcam, ab31263, 1:1,000, http://www.abcam.com/HDAC1-antibody-1T9-ChIP-Grade-ab31263.html), anti-SIRT1 (Abcam, ab7343, 1:1,000, http://www.abcam.com/sirt1-antibody-ab7343.html), anti-γH2AX (Millipore, 05-636, 1:1,000, http://www.millipore.com/catalogue/item/05-636) and anti–Flag M2 (Sigma, F1804, 1:1,000, http://www.sigmaaldrich.com/catalog/product/sigma/f1804?lang=en&region=US). Antibodies used for western blots were as follows: anti–Flag M2 (Sigma, F1804, 1:1,000), anti–c-Myc 9E10 (Thermo, MA1-980, 1:1,000, http://www.pierce-antibodies.com/c-Myc-antibody-clone-9E10-Monoclonal--MA1980.html), anti-HDAC1 (Thermo, PA1-860, 1:1,000, http://www.pierce-antibodies.com/HDAC1-antibody-Polyclonal--PA1860.html), anti–Sir2-α (Millipore, 07-131, 1:1,000, http://www.millipore.com/catalogue/item/07-131), anti–acetyl-lysine (Millipore, 05-515, 1:500, http://www.millipore.com/catalogue/item/05-515), anti-HA (Millipore, ab3254, 1:1,000, http://www.millipore.com/catalogue/item/ab3254), anti-HDAC1 (Lys432Ac) (1:1,000, ref. 18), anti-pATM (Ser1981) (Abcam, ab36810, 1:1,000, http://www.abcam.com/atm-phospho-s1981-antibody-10h11e12-ab36810.html) and anti-ATM (Abcam, ab2618, 1:1,000, http://www.abcam.com/atm-antibody-5c2-ab2618.html). Antibodies used for ChIP and immunoprecipitation experiments were all used at an amount of 2 μg per reaction and were as follows: anti–histone H4, pan (Millipore, 04-858, http://www.millipore.com/catalogue/item/04-858), anti-pATM (Ser1981) (Abcam, ab36810), anti-HDAC1 1.T9 (Abcam, ab31263), anti-NBS1 (Novus, NB100-60654, http://www.novusbio.com/NBS1-Antibody_NB100-60654.html), anti–Sir2-α (Millipore, 07-131) and anti–Flag M2 (Sigma, F1804).

Cell culture and transfection and infection. The cell lines used for experimentation were either HE293T cells (ATCC, CRL-11268) or an immortalized mouse hippocampal cell line (HT22)[39]. All cell lines were maintained in Dulbecco's Modified Eagle Media (DMEM; Gibco, 10566) supplemented with L-glutamine (5 mM), penicillin and streptomycin and fetal bovine serum. For live-imaging experiments, phenol red–free DMEM (Gibco, 31053) was used as a medium substitute. Cell lines were maintained at standard environmental conditions (97% humidity, 5% CO_2, 37 °C).

For primary neurons, dissociated cortical neurons dissected from embryonic day 16–18 Swiss-Webster mice were plated at a density of 500,000 cells per well in 24-well plates, 2 million cells per plate in 35-mm glass bottom plates and 15 million cells per plate in 10-cm plates. The plates were coated beforehand by incubation with poly-D-lysine (0.05 mg ml^{-1}) and laminin (0.005 mg ml^{1}) for 1 h at 37 °C followed by washing twice with dH_2O. Neurons were maintained in neurobasal medium (Gibco, 21103) supplemented with L-glutamine (5 mM), penicillin and streptomycin and B27 neuronal additive. Phenol red–free neurobasal medium (Gibco, 12348) was used as a substitute for the neuron cultures used in live-imaging experiments.

Cell lines and primary neuron cultures were transiently transfected using Lipofectamine 2000 reagent (Invitrogen, 11668) for at least 1 h in medium lacking antibiotics, after which cells were washed in warmed medium and given at least 24 h to allow for construct expression before usage. For live-imaging experiments using siRNA, 0.75 μg siRNA was cotransfected with either HDAC1-EmGFP or EmGFP-SIRT1 and given 48 h to allow for sufficient knockdown before imaging. For viral gene transduction, the virus was added directly to the culture medium. I-PpoI–ER was induced by adding 4-hydroxytamoxifen (Sigma, H7904) to a final concentration of 1 μM and incubated for 6 h before fixation.

Western blotting and immunoprecipitation. For both primary neurons and cell lines, 1.5–2 × 10^6 cells were washed once with PBS and lysed for 10 min on ice in RIPA buffer (150 mM NaCl, 1% IGEPAL, 0.5% NaDOC, 0.1% SDS and 50 mM Tris, pH 8.0, supplemented with protease inhibitors) on the plates in which they were originally grown. Cells were then collected by scraping and were rotated for 30 min at 4 °C. Supernatant was collected after centrifugation (13,000 r.p.m., 10 min, 4 °C). For each sample, SDS protein loading buffer was added to 1× and boiled (95 °C, 10 min) before loading onto a 10% sodium dodecyl sulfate polyacrylamide gel electrophoresis (SDS-PAGE) gel. Gels were transferred to polyvinylidene fluoride membranes (200 mA constant current) and blocked with 3% bovine serum albumin (BSA) in PBS plus Tween-20 (PBS-T) for 1 h before application of primary antibodies. Membranes were visualized with either electrochemiluminescence and autoradiographic film detection or the LiCor Odyssey quantitative western imaging system.

For immunoprecipitations, 1 mg of total protein lysate was used for each condition and brought to a total volume of 500 μl with RIPA buffer. The appropriate antibody was then added, and the mixture was incubated on a rotator overnight at 4 °C. As required, protein A/G-conjugated agarose beads (GE Health Science, 17-5280/17-0618) or Flag M2 affinity gel (Sigma, A2220) were equilibrated with RIPA buffer, blocked overnight with 3% BSA and washed before adding to the samples. For all immunoprecipitations, a total volume of 30 μl of bead slurry was used per reaction mix. The reaction mixtures were incubated for 1 h at 4 °C, after which they were washed four times and denatured by boiling (95 °C, 10 min) in RIPA buffer containing 1× SDS sample buffer.

Immunostaining, image acquisition and analysis. For immunostaining, cells were fixed by incubating with 4% paraformaldehyde for 10 min at room temperature and incubated with blocking buffer (5% normal donkey serum and 0.3% Triton X-100 in PBS) for 1 h. Primary antibodies were diluted in blocking buffer and incubated with cells overnight at 4 °C. Primary antibodies were visualized using the appropriate secondary antibodies conjugated to Cy2, Cy3 and Cy5 fluorescent dyes (Jackson ImmunoResearch Laboratories Inc., 1:500, 711-545-152, 711-165-152, 715-485-150, 715-165-150). Images for all fixed cells were acquired on a Zeiss LSM510 laser-scanning confocal microscope and subsequently deconvolved using theoretical point spread functions generated in ImageJ along with the Tikhonov-Miller iterative image restoration algorithm, which was implemented in the DeconvolutionLab plug-in written for ImageJ[40]. To assess and analyze images in a quantitative and unbiased manner, CellProfiler automated image analysis software[41] was trained to measure the per-cell γH2AX signal from a minimum of 100 cells per condition for all imaging experiments. For experiments using tagged proteins, CellProfiler was trained to consider transfected cells exclusively for quantification. Colocalization was assessed using ICA computation, which highlights pixels either negatively or positively covarying between two input channels. A plug in implementing this technique has been written as a plug-in for ImageJ and is freely available for download (http://imagej.nih.gov/ij/plugins/mbf/).

doi:10.1038/nn.3460

Image processing and analysis for microirradiation live imaging. All data acquired from microirradiation time lapses were processed according to the iterative deconvolution strategy described above before analysis. Normalized relative fluorescence (I_{rel}) within the 2-μm^2 rectangular-strip ROI was quantified for each time point using a computation that compensates for both background signal and fluorescence loss due to observational bleaching[42]. $\tau_{1/2}$ values were extracted from I_{rel} values by first converting them into fractional fluorescence values as described previously[43], and Prism5 was then used to plot and fit curves to this data.

HDAC1 structural modeling and tertiary structure prediction. The I-TASSER (http://zhanglab.ccmb.med.umich.edu/I-TASSER/) computational protein structure prediction algorithm was used to generate a three-dimensional predicted model for HDAC1 (refs. 44,45). The mouse HDAC1 (NP_032254) amino acid sequence and the crystal structure from the ancient HDAC1 ancestor, HDLP (RCSB Protein Data Bank ID 1C3P)[46], were used as inputs for processing by the I-TASSER algorithm. Output structure coordinates were processed and formatted in PyMOL, and amino acids were color coded to correspond to the HDAC1 functional domain schematic.

***In vivo* drug administration.** Mice were administered oral doses of 30 mg per kg body weight SIRT1 activator (compound #10) for 4 weeks. Dosage determination was based on pharmacokinetic studies that optimized for brain penetrance and minimal side effects. Oral gavage was performed using 1.5-inch, curved, 20-gauge, stainless steel feeding needles with a 2.25-mm ball (Braintree Scientific). Twice-daily gavage treatments were performed between the hours of 8 a.m. to 10 a.m. and 4 p.m. to 7 p.m.

Microirradiation and live imaging. Microirradiation was performed as described previously[47] on 7 d *in vitro* mouse primary cortical neurons using a Zeiss LSM710 inverted laser scanning confocal microscope. Cells were maintained in a controlled and stable environment for the duration of the imaging sessions. At least 24 h were allowed in transfected cells for construct expression.

ChIP. For ChIP, 1.5×10^6 cells were subjected to a two-step dual crosslinking procedure as described previously[48,49]. Purified DNA was analyzed by quantitative PCR (qPCR) using a BioRad CFX-96 quantitative thermocycler and SsoFast EvaGreen Low-ROX qPCR SuperMix (BioRad). Data were analyzed using the $\Delta\Delta C_T$ method (Applied Biosystems).

Single-cell electrophoresis (comet) assays. Cultured primary neurons were treated with 5 μM etoposide for 1 h and either allowed to recover for 16 h or dissociated immediately using 0.025% trypsin–ethylenediaminetetraacetic acid (EDTA). Dissociated neurons were embedded in a thin layer of low-melting agarose (0.5%), lysed and subjected to single-cell gel electrophoresis under alkaline conditions[11].

***In vitro* binding and acetylation and deacetylation reactions.** For binding reactions, anti-Flag–conjugated agarose beads (Sigma) were resuspended in 100 μl binding buffer (50 mM Tris-HCl (pH 7.5 at 25 °C), 5 mM $MgCl_2$, 1 mM EDTA, 100 mM NaCl, 0.05% NP-40 and 10% glycerol). HDAC1-Flag and SIRT1-His (1 μg each) were combined in reaction buffer (50 mM Tris-HCl (pH 7.5 at 25 °C), 1 mM dithiothreitol (DTT), 137 mM NaCl, 2.7 mM KCl, 4 mM $MgCl_2$, 0.1 mM EDTA, 1 mM NAD^+ and 10% glycerol) and incubated at 37 °C for 1 h. Each reaction was then supplemented with 30 μl of bead slurry and 90 μl of binding buffer and incubated in a rotator overnight at 4 °C. The beads were then pelleted, washed, boiled in Laemmli SDS-PAGE loading dye and analyzed by SDS-PAGE. In the acetylation reactions (30 μl), 100 ng recombinant HDAC1-Flag was incubated together with recombinant p300-HA in a buffer containing 50 mM Tris (pH 8.0 at 25 °C), 1 mM DTT, 1 mM phenylmethanesulfonylfluoride (PMSF), 0.1 mM EDTA, 50 nM acetyl-CoA and 10% glycerol and was incubated at 30 °C for 1 h. For deacetylation reactions, acetylation reactions were first performed as described above, after which the reactions were supplemented with NaCl (137 mM final), KCl (2.7 mM final), $MgCl_2$ (4 mM final), NAD^+ (1 mM final) and recombinant SIRT1-His and incubated for 1 h at 37 °C. HDAC1 enzymatic activity was measured using a fluorimetric assay as described[50]. Before measuring HDAC1 activity, acetyl-CoA and NAD^+ in the reactions were removed through dialysis, and 5 mM nicotinamide was added to ensure SIRT1 inactivation.

Liquid chromatography–mass spectrometry analysis. Gel bands containing HDAC1 were excised and in-gel digested using a protocol previously described[51]. The tryptic peptides were solubilized in high-performance liquid chromatography (HPLC) buffer A (0.1% formic acid in water) and loaded onto a capillary HPLC column (10 cm, 75 μm inside diameter) self-packed with Jupiter C12 resin (Phenomenex). Samples were separated using a 90-min linear gradient of 5–30% HPLC buffer B (0.1% formic acid in acetonitrile) and analyzed by an LTQ Orbitrap Velos mass spectrometer (Thermo Fisher Scientific Inc.). The tandem mass spectrometry data were analyzed with the Mascot search engine (Matrix Science, v2.1) with a Mascot cutoff score of 10 and $P < 0.05$ and with subsequent manual verification. Label-free quantification was performed for each lysine acetylation site on the basis of peptide precursor ion intensity normalized by protein abundance ratios.

Statistical methods. Standard statistical methods consistent with previous reports using similar assays, techniques and methods were used to analyze all data[11,14,21,47]. No statistical methods were used to predetermine sample sizes, but our sample sizes were similar to those reported in previous publications[10,13,21]. Analysis of γH2AX intensity in CK-p25 and tau P301S mice after treatment with SIRT1 activator were performed blind to the conditions of the experiment. For most other analyses, data collection and analysis were not performed blind to experimental conditions. Data were collected and processed randomly and appropriately blocked. The data distributions were assumed to be normal, but this was not formally tested.

35. Montgomery, R.L. *et al.* Histone deacetylases 1 and 2 redundantly regulate cardiac morphogenesis, growth, and contractility. *Genes Dev.* **21**, 1790–1802 (2007).
36. Cheng, H.L. *et al.* Developmental defects and p53 hyperacetylation in Sir2 homolog (SIRT1)-deficient mice. *Proc. Natl. Acad. Sci. USA* **100**, 10794–10799 (2003).
37. Yang, X.J. & Seto, E. The Rpd3/Hda1 family of lysine deacetylases: from bacteria and yeast to mice and men. *Nat. Rev. Mol. Cell Biol.* **9**, 206–218 (2008).
38. Takamiya, K., Mao, L., Huganir, R.L. & Linden, D.J. The glutamate receptor–interacting protein family of GluR2-binding proteins is required for long-term synaptic depression expression in cerebellar Purkinje cells. *J. Neurosci.* **28**, 5752–5755 (2008).
39. Davis, J.B. & Maher, P. Protein kinase C activation inhibits glutamate-induced cytotoxicity in a neuronal cell line. *Brain Res.* **652**, 169–173 (1994).
40. Vonesch, C. & Unser, M. A fast thresholded landweber algorithm for wavelet-regularized multidimensional deconvolution. *IEEE Trans. Image Process.* **17**, 539–549 (2008).
41. Carpenter, A.E. *et al.* CellProfiler: image analysis software for identifying and quantifying cell phenotypes. *Genome Biol.* **7**, R100 (2006).
42. Dundr, M. & Misteli, T. Measuring dynamics of nuclear proteins by photobleaching. *Curr. Protoc. Cell Biol.* **Chapter 13**, Unit 13.5 (2003).
43. Snapp, E.L., Altan, N. & Lippincott-Schwartz, J. Measuring protein mobility by photobleaching GFP chimeras in living cells. *Curr. Protoc. Cell Biol.* **Chapter 21**, Unit 21.1 (2003).
44. Roy, A., Kucukural, A. & Zhang, Y. I-TASSER: a unified platform for automated protein structure and function prediction. *Nat. Protoc.* **5**, 725–738 (2010).
45. Zhang, Y. I-TASSER server for protein 3D structure prediction. *BMC Bioinformatics* **9**, 40 (2008).
46. Finnin, M.S. *et al.* Structures of a histone deacetylase homologue bound to the TSA and SAHA inhibitors. *Nature* **401**, 188–193 (1999).
47. Kruhlak, M.J., Celeste, A. & Nussenzweig, A. Monitoring DNA breaks in optically highlighted chromatin in living cells by laser scanning confocal microscopy. *Methods Mol. Biol.* **523**, 125–140 (2009).
48. Nowak, D.E., Tian, B. & Brasier, A.R. Two-step cross-linking method for identification of NF-κB gene network by chromatin immunoprecipitation. *Biotechniques* **39**, 715–725 (2005).
49. Zeng, P.Y., Vakoc, C.R., Chen, Z.C., Blobel, G.A. & Berger, S.L. *In vivo* dual cross-linking for identification of indirect DNA-associated proteins by chromatin immunoprecipitation. *Biotechniques* **41**, 694, 696, 698 (2006).
50. Haumaitre, C., Lenoir, O. & Scharfmann, R. Histone deacetylase inhibitors modify pancreatic cell fate determination and amplify endocrine progenitors. *Mol. Cell Bio.* **28**, 6373–6383 (2008).
51. Zhao, Y., Zhang, W. & White, M.A. Capillary high-performance liquid chromatography/mass spectrometric analysis of proteins from affinity-purified plasma membrane. *Anal. Chem.* **75**, 3751–3757 (2003).

Corrigendum: SIRT1 collaborates with ATM and HDAC1 to maintain genomic stability in neurons

Matthew M Dobbin, Ram Madabhushi, Ling Pan, Yue Chen, Dohoon Kim, Jun Gao, Biafra Ahononu, Ping-Chieh Pao, Yi Qiu, Yingming Zhao & Li-Huei Tsai

Nat. Neurosci.; **doi:10.1038/nn.3460; corrected online 26 July 2013**

In the version of this article initially published online, author Biafra Ahanonu's name was misspelled Ahononu. The error has been corrected for the print, PDF and HTML versions of this article.